

# Genetic algorithm demystified for cosmological parameter estimation

Reginald Christian Bernardo<sup>a,\*</sup>, Yun Chen<sup>b</sup>

<sup>a</sup>Asia Pacific Center for Theoretical Physics, Pohang 37673, Republic of Korea

<sup>b</sup>Department of Physics, National Changhua University of Education, Changhua 50007, Taiwan

---

## Abstract

Genetic algorithm (GA) belongs to a class of nature-inspired evolutionary algorithms that leverage concepts from natural selection to perform optimization tasks. In cosmology, the standard method for estimating parameters is the Markov chain Monte Carlo (MCMC) approach, renowned for its reliability in determining cosmological parameters. This paper presents a pedagogical examination of GA as a potential corroborative tool to MCMC for cosmological parameter estimation. Utilizing data sets from cosmic chronometers and supernovae with a curved  $\Lambda$ CDM model, we explore the impact of GA's key hyperparameters—such as the fitness function, crossover rate, and mutation rate—on the population of cosmological parameters determined by the evolutionary process. We compare the results obtained with GA to those by MCMC, analyzing their effectiveness and viability for cosmological application.

---

## 1. Introduction

Genetic algorithm (GA) is a biology-inspired optimization strategy that incorporates elements of natural evolution to identify the fittest solution from a pool of similarly selected individual solutions. As a powerful optimization method, GA is classified as a metaheuristic because it does not rely on derivatives to find the optimum. Under certain conditions, it guarantees the best solution, even overcoming challenges posed by local optimality [1]. This method has been applied to a wide range of scientific problems, such as high energy physics [2] and gravitational wave astronomy [3]. GA is known for its ability to find the global optimum and distinguish tiny differences between seemingly similar solutions. It is particularly effective in navigating complex, high-dimensional parameter spaces and multimodal functions. In cosmology, it was introduced to overcome biases in selecting a cosmological model for inferring the properties of dark energy [4]. This approach was further developed by [5] and [6], which promoted GA as an alternative tool for cosmological analysis through uncertainty estimation. An excellent recent introduction to GA for cosmological parameter estimation can be found in [7].

On one hand, cosmology is currently a field facing significant challenges, necessitating a reevaluation of its foundational theories and analytical methods due to several persistent tensions in its fundamental parameters [8–12]. Notable among these is the Hubble tension [10], which refers to the discrepancy between the Hubble constant values derived from early universe observations (such as the cosmic microwave background [13]) and those obtained from local universe measurements [14]. Another critical issue is the tension in the amplitude of the smoothed matter power spectrum, which affects our understanding of large-scale structure formation [11]. These discrepancies suggest potential gaps or inaccuracies in our cosmological models and motivate the search for more robust analytical tools. In this context, GA, with its ability to navigate complex, high-dimensional parameter spaces and identify global optima, appears to be a promising approach. While not intended to replace traditional methods like Markov Chain Monte Carlo (MCMC), GA can complement them by providing alternative solutions and insights.

Our work provides a detailed and pedagogical exploration of the intricacies of GA for cosmological applications, using parameter estimation in the standard  $\Lambda$ CDM cosmological model as a medium of instruction. We focus specifically on the influences of key GA hyperparameters—fitness function, mutation, and crossover—on the output

---

\*Corresponding author

Email addresses: reginald.bernardo@apctp.org (Reginald Christian Bernardo), s0823042@gm.ncue.edu.tw (Yun Chen)

population of GA. By systematically examining these components, our study aims to clarify the role each one plays in GA and optimization for cosmological parameter estimation. This analysis is crucial for understanding how different settings and configurations can impact the efficiency and accuracy of GA in exploring cosmological parameter spaces. Additionally, our work demonstrates how GA can complement traditional methods, such as MCMC, by offering alternative pathways to finding optimal solutions [8]. Through this comprehensive approach, we aim to provide valuable guidance for researchers looking to apply GA in their cosmological investigations, thereby enhancing the toolkit available for addressing some of the field's most persistent challenges.

We proceed by first introducing the data sets and cosmological model considered for our analysis (Section 2). Then, we review MCMC and GA (Section 3). We present our main results in Section 4, emphasizing the exploration of GA hyperparameter space to achieve an optimal evolved population, in contrast with only a single best solution. We also touch on the comparison between GA and MCMC (Section 4.4), setting a baseline for further calibrating GA for cosmological parameter estimation in par with MCMC. We conclude by discussing potential further applications of GA in cosmology and extensions of this work.

## 2. Cosmology: model and data sets

We consider background cosmological data from cosmic chronometers (CC) [15–21] and supernovae (SNe) [22–24], described below within the framework of a spatially curved  $\Lambda$ CDM model.

*Cosmic Chronometers*—The CC are best thought of as cosmic standard clocks; due to their inherent capability to give a direct account of the expansion rate of the Universe at late times [15, 19, 20, 25, 26],  $z \lesssim 2$ . The main idea is that the expansion rate at a redshift  $z_{CC}$  can be estimated through the difference in the ages of redshift-adjacent galaxies, playing on an age-ladder analogous to the usual distance-ladder. Thus, to a good approximation, the expansion rate at a redshift  $z_{CC}$  can be written as  $H_{CC} \approx -(\Delta z_{CC}/\Delta t) / (1 + z_{CC})$ , where  $\Delta t$  and  $\Delta z_{CC}$  are deduced from the differences in the age and metallicity of temporally-adjacent-passive galaxies. This is a most direct way to observe the cosmic expansion. For our purposes, we consider the CC in the redshift range  $0.07 \lesssim z \lesssim 1.97$  that is compiled in [27].

We describe the cosmology underlying CC as a curved  $\Lambda$ CDM cosmological model; where the normalized Hubble expansion rate,  $E(z) = H(z)/H_0$ , is given by

$$E(z)^2 = \Omega_{m0}(1+z)^3 + \Omega_{k0}(1+z)^2 + (1 - \Omega_{m0} - \Omega_{k0}), \quad (1)$$

and  $H_0$  is the Hubble constant,  $\Omega_{m0}, \Omega_{k0}$  are the energy fractions/density parameters corresponding to nonrelativistic matter and curvature at redshift  $z = 0$ . The present dark energy fraction is given by  $\Omega_{de0} = 1 - \Omega_{m0} - \Omega_{k0}$ , the last term in the parenthesis on the right hand side in (1). The likelihood of this model compared with the data,  $H_{CC}(z_{CC}) \pm \Delta H_{CC}(z_{CC})$  at  $z_{CC}$ , can be written as

$$\log \mathcal{L}_{CC} \propto -\frac{1}{2} \sum_{z_{CC}} (H(z_{CC}) - H_{CC}(z_{CC})) C_{CC}^{-1} (H(z_{CC}) - H_{CC}(z_{CC})), \quad (2)$$

where  $C_{CC}$  is the covariance matrix of correlated CC measurements [27].

*Supernovae*—Type Ia SNe are intrinsically very bright objects, historically serving as one of cosmology's most reliable distance indicators [28–34]; for this reason, they have been thought of as cosmic standard candles, serving like lighthouses in the sky that indicate distances relative to an observer, assuming that the intensity of the source declines according to the inverse square law. Their high brightness and flux particularly facilitate standardization, meaning that by calibrating the flux measurements relative to a host, one can construct a rigorous distance-redshift ladder. This ladder accounts for the Universe's expansion rate through its perceived effect on the brightness of SNe. This distance ladder can be written as

$$\mu(z) = 5 \log_{10}(d_L(z)) + 25, \quad (3)$$

where  $\mu(z) = m(z) - M$  is the distance modulus, representing the difference between the apparent  $m(z)$  and intrinsic  $M$  magnitudes of SNe at a redshift  $z$ , and  $d_L(z)$  is the luminosity distance, estimated through flux measurements,  $F = L/(4\pi d_L^2)$  with  $L$  being the luminosity. For this work, we use the Pantheon+ SNe compilation [22–24], utilizing measurements in the redshift range  $0.01 \lesssim z \lesssim 2.3$  to avoid possible bias from galaxy peculiar velocities, among other effects, at very low redshifts  $z < 0.01$  [35, 36].

As in CC, we attribute the cosmology underlying SNe observations to a curved  $\Lambda$ CDM model. In this case, the luminosity distance is given by

$$d_L(z) = (1+z) \frac{c}{H_0 \sqrt{\Omega_{k0}}} \sin \left( H_0 \sqrt{\Omega_{k0}} \int_0^z \frac{dz'}{E(z')} \right), \quad (4)$$

where  $c$  is the speed of light in vacuum and the normalized expansion rate  $E(z)$  is given by (1). We associate this model to the data via the likelihood

$$\log \mathcal{L}_{\text{SNe}} \propto -\frac{1}{2} \sum_{z_{\text{SNe}}} (\mu(z_{\text{SNe}}) - \mu_{\text{SNe}}(z_{\text{SNe}})) C_{\text{SNe}}^{-1} (\mu(z_{\text{SNe}}) - \mu_{\text{SNe}}(z_{\text{SNe}})), \quad (5)$$

where  $C_{\text{SNe}}$  is the covariance matrix [22–24].

Figure 1 shows the data sets considered in this work together with predictions of the curved  $\Lambda$ CDM model.

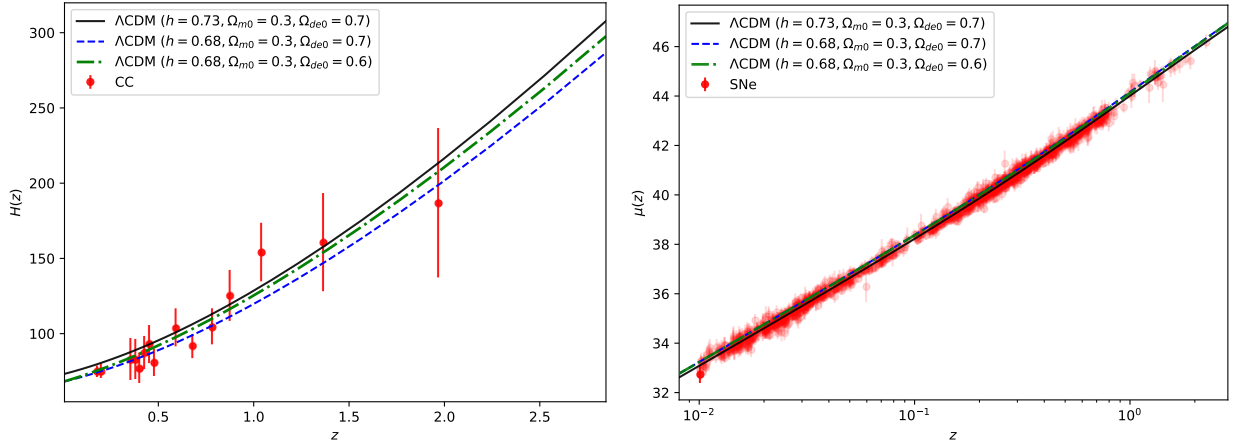


Figure 1: [Left] Expansion rate from CC [27] and [right] distance moduli from SNe [22–24] with curved  $\Lambda$ CDM predictions (1) and (3). Note that  $h = H_0/100 \text{ km s}^{-1} \text{ Mpc}^{-1}$  and  $\Omega_{de0} = 1 - \Omega_{m0} - \Omega_{k0}$ .

We emphasize that in practice there can be several models that are well suited to fit the same data sets. For this work, we shall not be concerned with model selection and hypothesize that curved  $\Lambda$ CDM is suitable to describe CC and SNe, such that its parameters can be constrained by MCMC and GA.

### 3. MCMC and genetic algorithm

We introduce GA in this section through the eyes of MCMC, by first providing an overview of the traditional method, and then following up with a detailed account of GA.

#### 3.1. MCMC

MCMC methods, grounded in Bayesian statistics, are powerful tools for exploring complex parameter spaces through random sampling. By utilizing a Markovian property, where the current state depends only on the immediate preceding state, MCMC facilitates efficient navigation of high-dimensional probability distributions toward a local solution, well approximated by a posterior [37–39].

Given a data set  $D$  and parameters  $p$  of a model  $M$ , Bayes' theorem provides the framework for incrementally improving our estimates of  $p$  based on observed data:

$$P(p|D, M) = \frac{P(D|p, M)P(p|M)}{P(D|M)}, \quad (6)$$

where  $P(p|D, M)$  (posterior) is the probability distribution of the parameters  $p$  given  $D$  and  $M$ ;  $P(D|p, M)$  (likelihood) represents the probability of observing  $D$  for given  $p$  and  $M$ ;  $P(p|M)$  (prior) encodes prior knowledge about  $p$ ; and  $P(D|M)$  (evidence) acts as a normalizing constant. For cosmological parameter estimation, our focus is on computing the posterior distribution  $P(p|D, M)$ . Since we are not performing model comparison in this work, the evidence  $P(D|M)$  can be treated as a constant.

Among numerous MCMC algorithms, the Metropolis-Hastings method remains one of the simplest and most widely used. It constructs a Markov chain that converges to the target posterior distribution. The iterative procedure involves: (1) starting at the current position  $X(t)$ , a new candidate position  $Y$  is proposed from a transition distribution  $Q(Y; X(t))$ ; and (2) the candidate position is accepted with probability:

$$\min\left(1, \frac{P(Y|D, M)}{P(X(t)|D, M)} \frac{Q(X(t); Y)}{Q(Y; X(t))}\right). \quad (7)$$

If  $Y$  is accepted, the chain moves to  $Y$ , setting  $X(t+1) = Y$ ; otherwise, it remains at  $X(t)$ , so  $X(t+1) = X(t)$ . This ensures that the chain samples according to the posterior distribution in the long run.

The choice of the transition distribution  $Q(Y; X(t))$  is critical for the efficiency of the Metropolis-Hastings algorithm. A common and practical choice is a multivariate Gaussian distribution centered at  $X(t)$ , with a covariance matrix carefully tuned for optimal performance. This ensures a balance between exploration and convergence. Poorly chosen transition distributions may result in slow convergence or inefficient sampling. Adaptive methods that adjust the covariance matrix dynamically during the sampling process have proven effective in improving performance in high-dimensional spaces.

For this work, we consider flat priors and the likelihoods of CC (2) and SNe (5) described in Section 2. We use the public code `emcee` to perform MCMC [40].

### 3.2. Genetic algorithm

GA belongs to the broader class of Evolutionary Algorithms, which optimize populations of solutions rather than focusing solely on individual candidates [8]. This population-based approach has found diverse applications across fields, including high-energy physics and gravitational wave astronomy [2, 3]. In cosmology, GA was first introduced to mitigate biases in model selection, particularly for analyzing dark energy models [4]. Since then, it has proven effective in a variety of tasks, such as estimating cosmological parameter uncertainties [5, 6], selecting kernel functions in Gaussian process regression [41], optimizing neural network architectures [42], enhancing spectroscopic modeling [43–45], and aiding model selection with information criteria [46]. We refer readers to [7, 8] for a recent review of GA’s applications in cosmological parameter estimation and reconstruction.

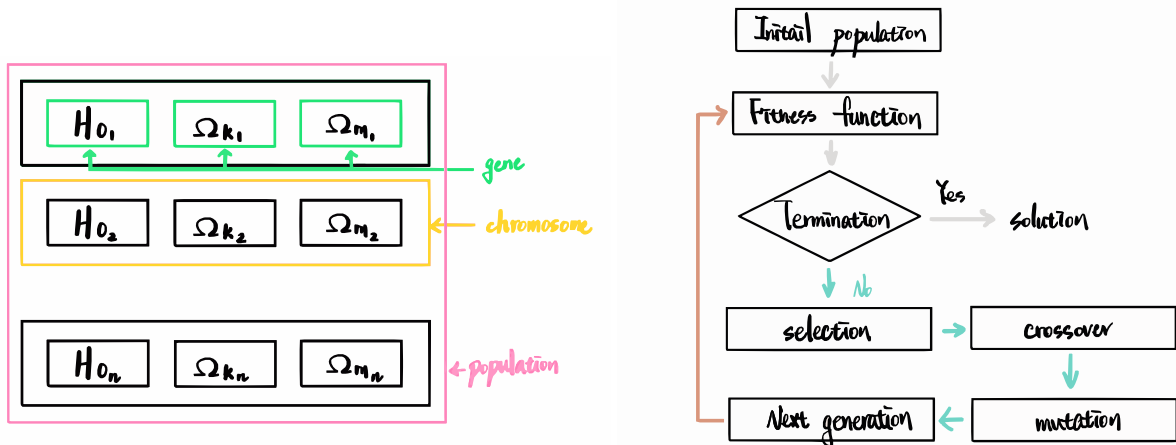


Figure 2: [Left] Anatomy of a population in GA and [right] GA’s flowchart.

GA simulates the process of natural selection in biological evolution. By employing mechanisms such as inheritance, crossover, mutation, and selection, GA iteratively evolves a population of solutions toward an optimal

result (Figure 2). Unlike methods like MCMC, which excel in local searches, GA performs global searches across the parameter space, making them particularly suitable for high-dimensional and multimodal optimization problems. However, their effectiveness comes at a computational cost, as they are sensitive to parameter settings, and improperly tuned parameters can lead to suboptimal convergence or stagnation in local minima.

In comparison to MCMC, GA excels in exploring a broader search space but require careful parameter tuning and greater computational resources. While MCMC relies on localized random walks to converge to a posterior distribution, GA maintains and evolves a population of solutions, increasing the chances of finding global optima. However, this advantage is counterbalanced by challenges such as determining appropriate population sizes, mutation rates, and crossover probabilities, which often require extensive experimentation. Adaptive techniques can partially address these issues, ensuring efficient exploration without compromising convergence speed.

The workflow of a GA involves several stages (Figure 2), each inspired by biological evolution:

*Initialize population*—A population of candidate solutions, or chromosomes, is randomly generated. Each chromosome represents a potential solution, where its genes correspond to parameters like  $H_0$ ,  $\Omega_m$ , and  $\Omega_k$  in cosmological applications.

*Fitness calculations*—The fitness function quantifies the quality of each chromosome. In this work, we use statistical measures such as the log-likelihood (8), an inverse chi-square (9), and the likelihood (10) to evaluate fitness.

*Selection*—In roulette wheel selection, chromosomes are chosen based on their fitness. Higher fitness chromosomes occupy larger sections of the wheel, increasing their chances of being selected for the next generation.

*Crossover*—Pairs of selected chromosomes exchange genetic information to produce offspring. We employ a scattered crossover method, which randomly selects crossover points between parent chromosomes to preserve diversity while fostering convergence.

*Mutation*—To maintain genetic diversity, random mutations are introduced into the population. Adaptive mutation, where the mutation rate depends on the population’s overall fitness, ensures effective exploration during early generations and stabilizes convergence in later stages.

For this work, we shall play with the fitness function, crossover and mutation rates to assess their impacts on the population. We use the public code pyGAD to perform GA [47].

## 4. Results and Discussion

In this section, we present our results, playing with the key parameters of GA (fitness function, cross-over, mutation) and studying their influence on the final evolved population, of  $\Lambda$ CDM cosmological parameters.

### 4.1. Fitness function

We begin our discussion with GA’s most important ingredient, the fitness function. To understand its impact on the parameter estimation, we consider three different functional forms, all depicting a distance measurement between the data and the model prediction; we take

$$\text{FF}_1 = -\chi^2/2, \quad (8)$$

$$\text{FF}_2 = 100/\chi^2, \quad (9)$$

$$\text{FF}_3 = \exp(-\chi^2/2), \quad (10)$$

where  $\chi^2 = -2 \log \mathcal{L}$  and  $\mathcal{L}$  is the likelihood, (2) for CC and (5) for SNe. The common denominator between these different forms are that closer distances (between data and model;  $\chi^2 \lesssim 1$ ) give more positive values of the fitness. We feed each fitness function into GA, with an initial uniform prior on the cosmological parameters, and see where the evolution in 100 generations take the population. Throughout, we consider a fixed population size of 3000, a ‘roulette wheel’ selection with a fixed selection rate of 30%, a ‘scattered’ crossover with a fixed probability of 50%, and an adaptive mutation rate, mutating a fraction 30% of the genes of high quality solutions and a fraction 50% of the genes of low quality solutions. The evolved population are shown in Figure 3 after 100 generations.

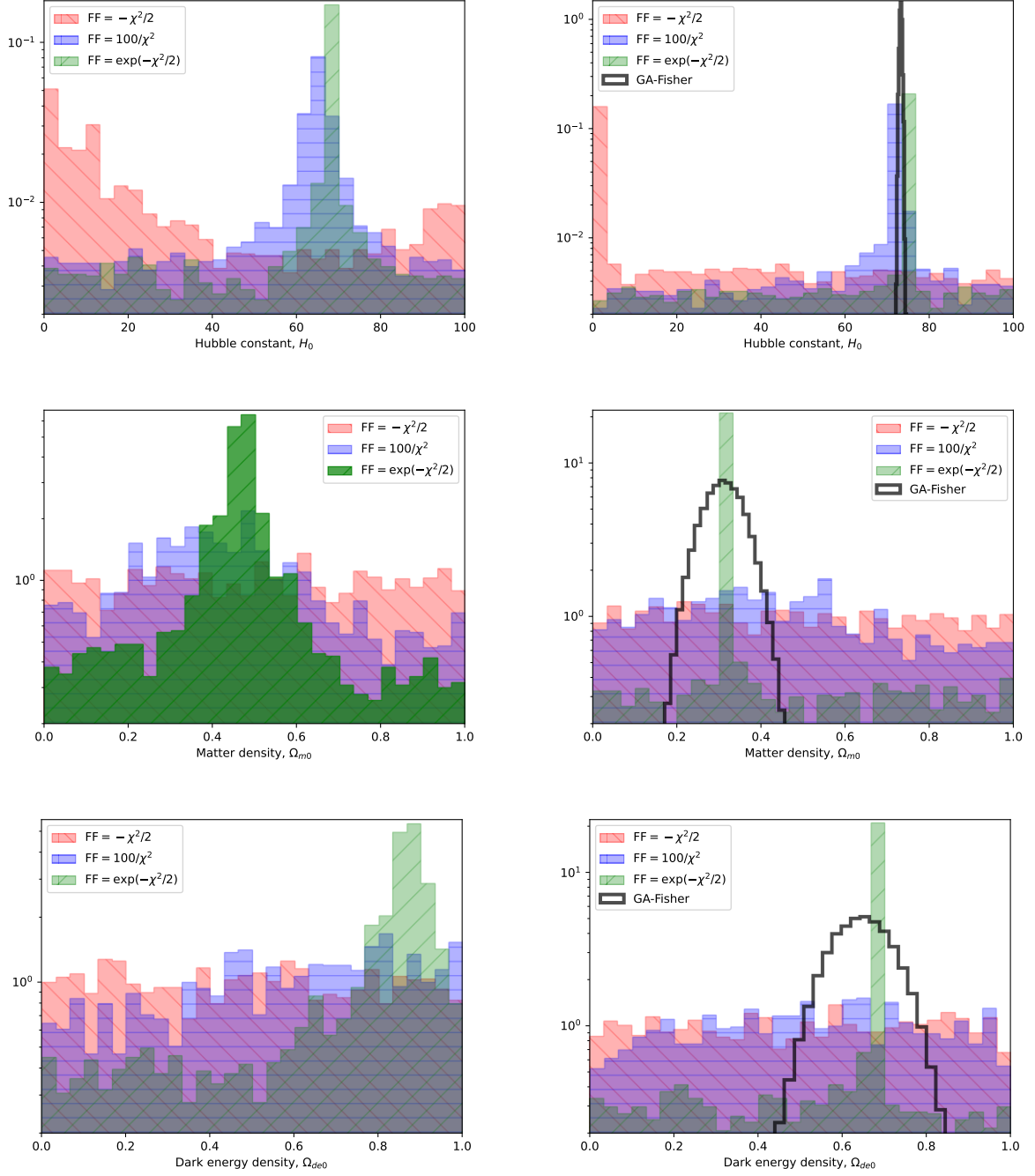


Figure 3: Changing fitness—GA final population distribution for different fitness functions;  $FF = -\chi^2/2$ ,  $100/\chi^2$ ,  $\exp(-\chi^2/2)$  with fixed mutation (0.5,0.3) and crossover (50%) rates. (left column) results obtained with only CC data (right column) results with CC and SNe. In the right column, the Gaussian (GA-Fisher) corresponds to the GA best solution compounded with a Fisher matrix uncertainty estimate based on the likelihood.

Results show that the choice of the functional form of the fitness function has a significant impact to the final evolved population. Focusing on CC results (left column of Figure 3), we realize this in each one of the cosmological parameters,  $H_0$ ,  $\Omega_{m0}$ , and  $\Omega_{de0}$ , where each population basically turns out flat with  $FF_1$ . It is worth noting that



we present the histogram frequencies in log-scale in order to highlight the differences between the results of fitness functions (8-10), which otherwise would have been more difficult to perceive visually in linear scale. On the other hand, using  $FF_2$  gets the final evolved population to be a bit more localized, in the usual way cosmological parameter estimates are viewed. However, the population remains less localized than desired for this purpose. Moving forward to  $FF_3$ , we find that the last evolved population has turned out quite localized, narrowed to the place where we expect the bulk of the cosmological parameters inferred via MCMC (to be confirmed in Section 4.4).

The addition of SNe data supports the results obtained with CC data on the importance of picking out a suitable fitness function. Using the same set of fixed GA parameters, we perform the GA with fitness functions (8-10). The results after 100 generations are shown in the right column of Figure 3.

This shows that the fitness function  $FF_1$  leads to a flat final population (parameter distribution) despite all the operations and evolution in GA; while  $FF_2$  leads to kind of the same uniform distribution, except for  $H_0$  which somehow turns out localized. This suggests that the addition of the more stringent supernovae data is insufficient to help GA get out of the initial uniform population distribution. However, the fitness function  $FF_3$  completely amends this, in all cases resulting to a quite localized distribution of parameters after 100 generations. The best GA solution almost always belongs to this localized set in the final population. The impact of the addition of SNe on the width of the localized set per parameter is also highly notable.

#### 4.2. Mutation

We next explore the impact of mutation (or rather the mutation rate) on the final evolved population in GA. Following the lessons of the previous section, we fix the fitness function to be  $FF_3$  (10), and consider two choices for an adaptive mutation rate of  $m_1 = (50\%, 30\%)$  and  $m_2 = (80\%, 30\%)$ . The first choice  $m_1$  means that half of the chromosomes of a gene are going to be tweaked by mutation for low quality solutions; while 30% of the chromosomes will be altered for high quality solutions. The same interpretation extends to our second choice  $m_2$ . Ideally we want the first percentage in the input tuple to be higher such that low quality solutions mutate more. In addition to a fixed fitness function, we consider a fixed population size of 3000, a roulette wheel selection with a fixed selection rate of 30%, and a scattered crossover with a fixed probability of 50%. The evolved population are shown in Figure 4 after 100 generations.

Our results suggest that higher mutation rates also lead to more localized populations after evolution. To get to this, we start with the CC results (left column of Figure 4). In this case, we find that the populations resulted from the higher mutation  $m_2$  are always a tad narrower compared with the populations outputted by  $m_1$ . Nonetheless, the peaks of the parameter space histograms resulted from both mutation rates coincide. The same conclusion can be drawn with the addition of SNe data (right column of Figure 4). The final populations per parameter have localized as expected due to the addition of a stringent data set. Consequently, the difference between the widths of the localized set of parameters in the final population has turned out to be less perceivable. In principle, there may still be a small difference. However, we expect that such minute difference will be completely hidden away by uncertainty, which we have yet to return to (in Section 4.4).

Our results support that higher mutations can have help in producing a localized set of parameters in the final evolved population.

#### 4.3. Crossover

We lastly explore the crossover rate's impact in GA. Analogous to the previous sections, we fix the fitness function to  $FF_3$  (10), and consider a population size of 3000, a roulette wheel selection with a fixed selection rate of 30%, and an adaptive mutation rate probability of  $m_1 = (50\%, 30\%)$ . We note that we could have similarly chosen  $m_2$  as long as the mutation rate is fixed so that the results can attributed to changes in other variables. We consider three crossover scenarios, one with  $c_1 = 50\%$ ,  $c_2 = 80\%$ , and  $c_3 = 30\%$ . In GA, the scattered crossover mechanism combines genes from two parents based on a randomly generated binary mask. With a  $c_i$  crossover probability, there is a  $c_i$  chance that the crossover will occur, meaning new offspring are produced less frequently, often resulting in offspring that closely resemble one of the parents. The results obtained for each crossover  $c_{1-3}$  are shown in Figure 5.

This shows that crossover is less of a factor compared with the fitness function and the mutation rate for the localized set of parameters in the final population. One way we can understand this is through definition; crossover is the process by which the gene pool is mixed up in a population in order to increase diversity. We find that this does

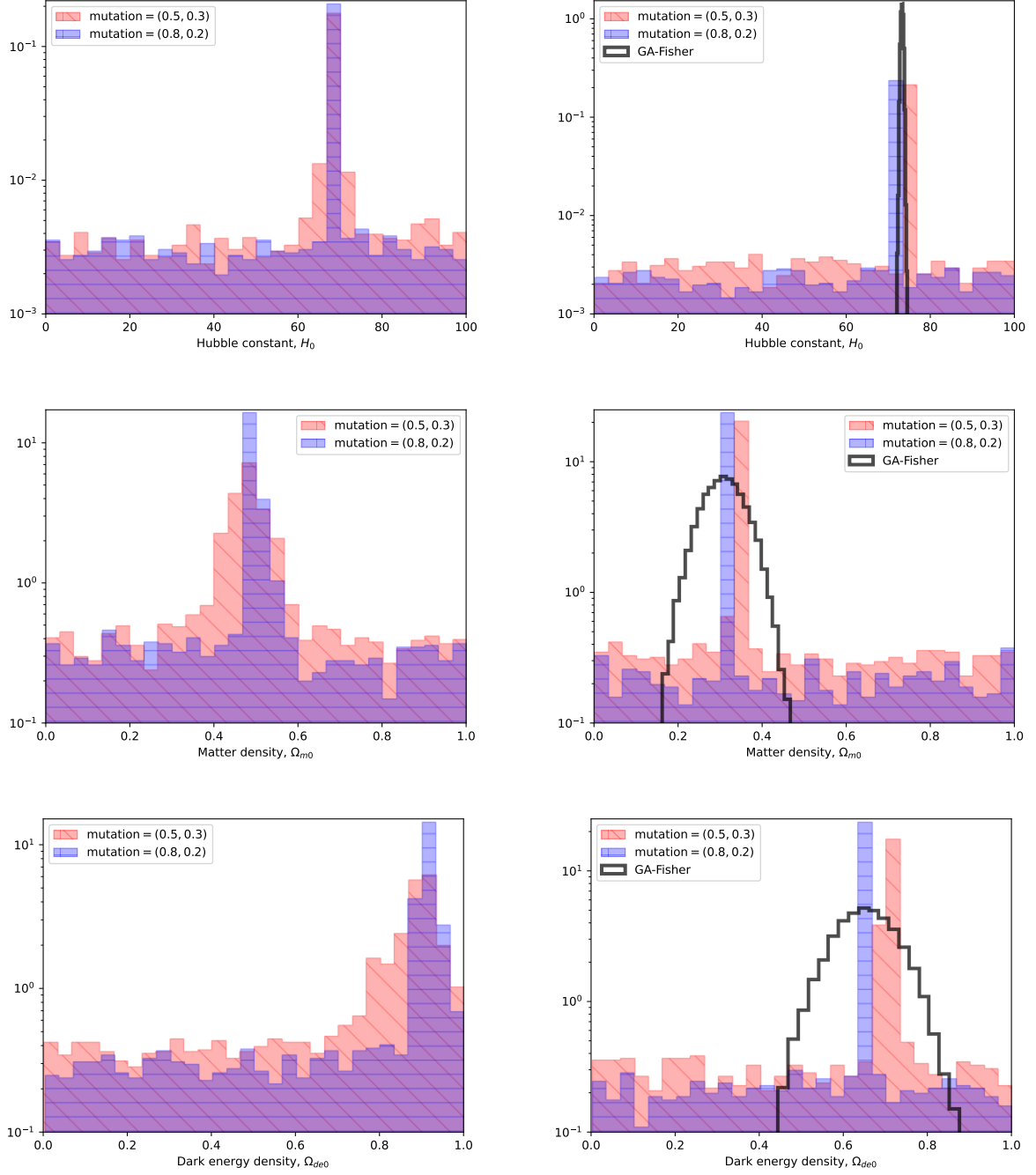


Figure 4: Changing mutation—GA final population distribution for different mutation rates; mutation=(0.5, 0.3), (0.8, 0.2) with fixed fitness function  $\exp(-\chi^2/2)$  and crossover rate (50%). In the right column, the Gaussian (GA-Fisher) corresponds to the GA best solution compounded with a Fisher matrix uncertainty estimate based on the likelihood.

not produce perceivable influences to the final population regardless of the choice. Results with CC alone and with both CC and SNe support this statement. Figure 5 suggests that the choice of the crossover probability has less impact on the cosmological parameter space, i.e., the final populations for each parameter are barely distinguishable and the



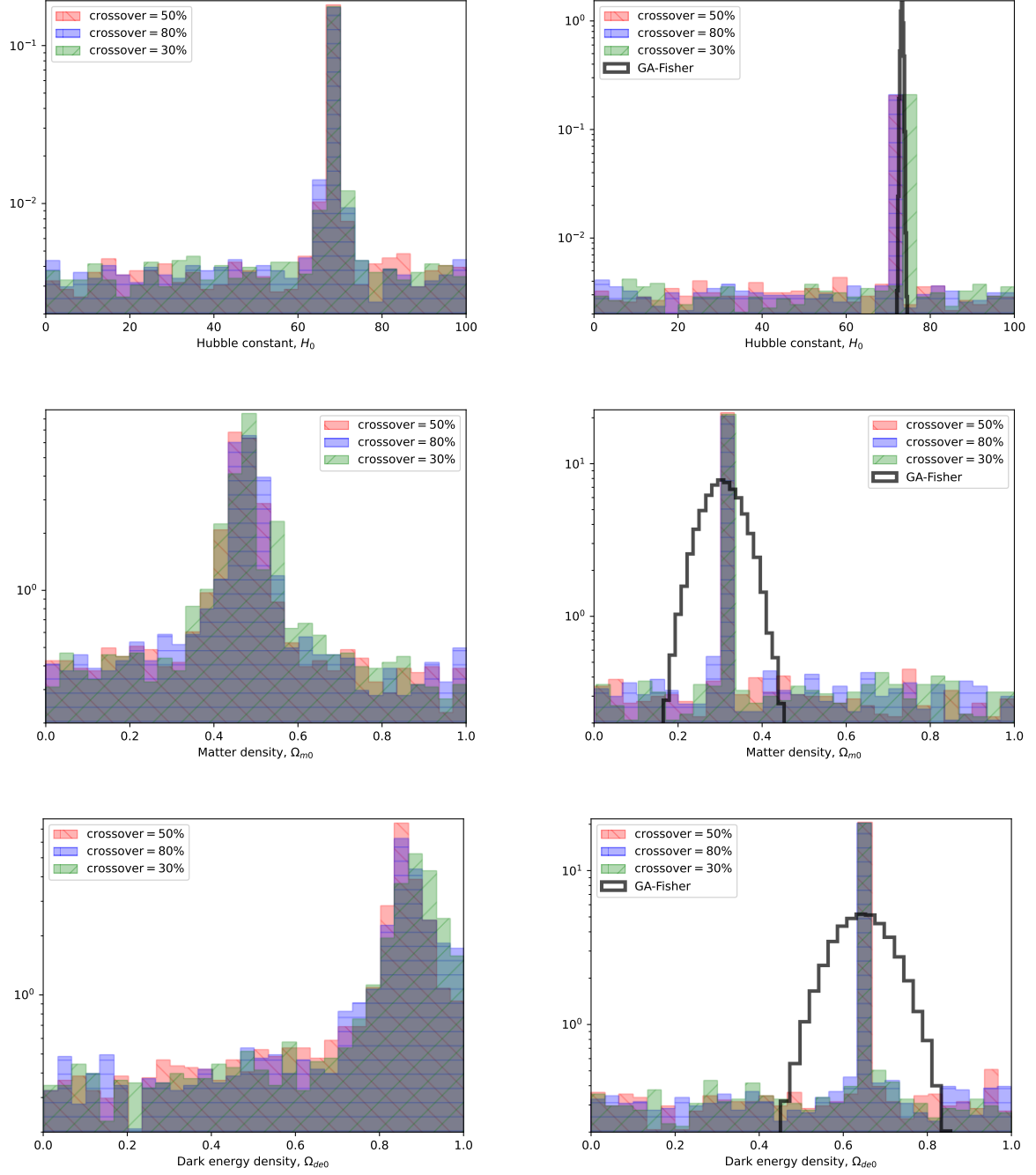


Figure 5: Changing crossover—GA final population distribution for different crossover rates; crossover=50%, 80%, 30% with fixed fitness function  $\exp(-\chi^2/2)$  and mutation rate (0.5, 0.3). In the right column, the Gaussian (GA-Fisher) corresponds to the GA best solution compounded with a Fisher matrix uncertainty estimate based on the likelihood.

uncertainty would only obscure small differences, if any. Admittedly, in the top right of Figure 5 the Hubble constant distribution has notably shifted by a bin for the low crossover probability. This change is irrelevant, and we view our statement on the impact of the crossover probability as a rule of thumb.

#### 4.4. Discussion

It is worth noting that the parameter distributions obtained from GA are highly localized and non-Gaussian, regardless of the values of the hyperparameters. We could nonetheless take it as an exercise for illustrative purposes to blindly treat the final population as if it were a posterior. In this way, we can look at the marginalized statistics of the GA samples, comparing the results with a corresponding MCMC analysis (Section 3.1). The results are shown in Table 1.

Table 1: GA constraints (68% confidence intervals) on the cosmological parameters of curved  $\Lambda$ CDM.  $H_0$  are given in units  $\text{km s}^{-1}\text{Mpc}^{-1}$ ; fitness functions  $\text{FF}_i$  are given by (8-10); mutation rates are  $m_1 = (50\%, 30\%)$ ,  $m_2 = (80\%, 20\%)$ ; crossover probabilities are  $c_1 = 50\%$ ,  $c_2 = 80\%$ ,  $c_3 = 30\%$ .

| Data set | Method | Change                    | $H_0$                  | $\Omega_{m0}$                | $\Omega_{de0}$            |
|----------|--------|---------------------------|------------------------|------------------------------|---------------------------|
| CC       | GA     | Fitness ( $\text{FF}_1$ ) | $20.2^{+59.0}_{-17.2}$ | $0.5^{+0.3}_{-0.3}$          | $0.5^{+0.3}_{-0.3}$       |
|          |        | Fitness ( $\text{FF}_2$ ) | $64.3^{+6.8}_{-26.7}$  | $0.4^{+0.3}_{-0.2}$          | $0.6^{+0.3}_{-0.4}$       |
|          |        | Fitness ( $\text{FF}_3$ ) | $67.8^{+1.6}_{-23.2}$  | $0.5^{+0.1}_{-0.1}$          | $0.8^{+0.1}_{-0.4}$       |
|          |        | Mutation ( $m_1$ )        | $68.3^{+1.1}_{-19.5}$  | $0.5^{+0.1}_{-0.1}$          | $0.9^{+0.1}_{-0.4}$       |
|          |        | Mutation ( $m_2$ )        | $68.1^{+0.8}_{-15.0}$  | $0.49^{+0.04}_{-0.03}$       | $0.91^{+0.02}_{-0.36}$    |
|          |        | Crossover ( $c_1$ )       | $67.9^{+1.5}_{-22.4}$  | $0.5^{+0.1}_{-0.1}$          | $0.8^{+0.1}_{-0.4}$       |
|          |        | Crossover ( $c_2$ )       | $67.6^{+2.0}_{-24.3}$  | $0.5^{+0.1}_{-0.1}$          | $0.8^{+0.1}_{-0.4}$       |
|          |        | Crossover ( $c_3$ )       | $67.8^{+2.0}_{-23.6}$  | $0.5^{+0.1}_{-0.1}$          | $0.9^{+0.1}_{-0.4}$       |
|          | MCMC   |                           | $65 \pm 6$             | $0.4 \pm 0.2$                | $0.6 \pm 0.3$             |
| CC+SNe   | GA     | Fitness ( $\text{FF}_1$ ) | $0^{+65}_{-0}$         | $0.5^{+0.4}_{-0.3}$          | $0.5^{+0.3}_{-0.4}$       |
|          |        | Fitness ( $\text{FF}_2$ ) | $71.9^{+1.3}_{-23.7}$  | $0.4^{+0.3}_{-0.3}$          | $0.5^{+0.3}_{-0.3}$       |
|          |        | Fitness ( $\text{FF}_3$ ) | $73.4^{+0.0}_{-21.4}$  | $0.320^{+0.148}_{-0.001}$    | $0.7^{+0.0}_{-0.2}$       |
|          |        | Mutation ( $m_1$ )        | $73.4^{+0.0}_{-21.0}$  | $0.340^{+0.153}_{-0.002}$    | $0.7^{+0.0}_{-0.2}$       |
|          |        | Mutation ( $m_2$ )        | $73.3^{+0.0}_{-3.1}$   | $0.313^{+0.003}_{-0.000}$    | $0.7^{+0.0}_{-0.0}$       |
|          |        | Crossover ( $c_1$ )       | $73.2^{+0.0}_{-23.1}$  | $0.3120^{+0.1210}_{-0.0004}$ | $0.648^{+0.003}_{-0.134}$ |
|          |        | Crossover ( $c_2$ )       | $73.3^{+0.0}_{-22.6}$  | $0.3^{+0.2}_{-0.0}$          | $0.658^{+0.002}_{-0.145}$ |
|          |        | Crossover ( $c_3$ )       | $73.2^{+0.0}_{-19.9}$  | $0.3^{+0.2}_{-0.0}$          | $0.7^{+0.0}_{-0.2}$       |
|          | MCMC   |                           | $73.2 \pm 0.3$         | $0.3 \pm 0.1$                | $0.6 \pm 0.1$             |

These show the uncertainty estimates of the cosmological parameters in GA based on the final evolved population. As we alluded to already, the shape of the distribution of samples in the final population are generally non-Gaussian; an implication of this goes to the upper and lower confidence limits as shown in Table 1 which are highly influenced by prior on the parameter space being investigated. This can be understood solely due to the fact that GA is not meant to converge to a posterior, unlike MCMC; GA operations (selection, crossover, mutation) have been put in place to specifically prevent convergence in order to work well for global optimization, and it does the job well. This implies that there are always going to be outliers, residing outside the localized set of samples close to the true solution, no matter how tuned evolution is made to be. These outliers explain the huge variances in GA parameter estimation, since we used directly the evolved population for uncertainty estimation.

To elucidate on this point further, we investigate the combined CC and SNe data sets, using MCMC and GA, where for GA we also present the final evolved samples as well as uncertainty estimates using the Fisher matrix. Furthermore, taking in lessons learned earlier, we use an optimized hyperparameters in order to obtain a rather localized set of samples in the final population: fitness function  $\text{FF}_3$ , selection rate 30%, adaptive mutation rate  $m_2 = (80\%)$ , and crossover probability  $c_1 = 50\%$ . This catered a final population that is sharply concentrated at  $H_0 = 73.3 \text{ km s}^{-1}\text{Mpc}^{-1}$ ,  $\Omega_{m0} = 0.3$ ,  $\Omega_{de0} = 0.6$ , with no perceivable variation around it at the 68% confidence limit. The results are shown in Figure 6.

It is notable that the application of the Fisher matrix in conjunction with GA to provide an uncertainty band gives comparable results to MCMC [7]. This has been established in GA applications to grammatical evolution for

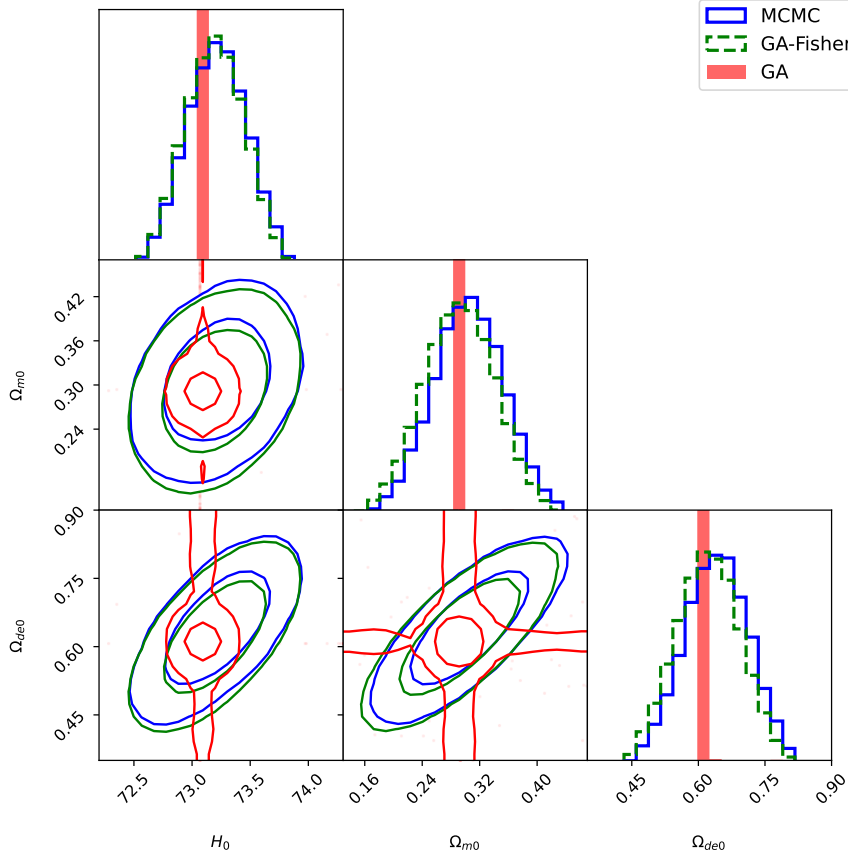


Figure 6: Constraints on curved  $\Lambda$ CDM with CC and SNe data obtained using MCMC and GA; MCMC (blue) results  $H_0 = 73.21^{+0.28}_{-0.28}$  km s $^{-1}$ Mpc $^{-1}$ ,  $\Omega_{m0} = 0.31^{+0.05}_{-0.05}$ ,  $\Omega_{de0} = 0.64^{+0.08}_{-0.08}$ . GA-Fisher (green) results  $H_0 = 73.24^{+0.27}_{-0.28}$  km s $^{-1}$ Mpc $^{-1}$ ,  $\Omega_{m0} = 0.32^{+0.05}_{-0.05}$ ,  $\Omega_{de0} = 0.65^{+0.08}_{-0.08}$ . GA (red) gives  $H_0 = 73.3$  km s $^{-1}$ Mpc $^{-1}$ ,  $\Omega_{m0} = 0.3$ ,  $\Omega_{de0} = 0.6$  (variation from the optimal solution is negligible).

the reconstruction of cosmological functions [5, 6], where other methods such as path integral approach for GA uncertainty estimation has also been explored. In this case, MCMC and the GA-Fisher matrix hybrid (GA-Fisher) have almost given the same constraints on the cosmological parameters, including the correlation in the parameters. See also [8]. However, we must warn that the GA-Fisher estimate cannot always be relied upon, particularly when there is a lack of data, such is the case when we consider only the CC data. This is the reason we did not display the GA-Fisher bands in the left panels of Figures 3-5, since the covariance estimates did not converge. This is completely understandable because the Fisher matrix uncertainty estimation is a forecasting approach. Hence, its reliability depends strongly on the amount of input it deals with. Nonetheless, the sheer size of the SNe data makes it a reliable alternative tool for cosmological parameter estimation together with GA, as shown in Figure 6. On the other hand, the GA samples can be used to gain more confidence in MCMC, as depicted in Figure 6 where the GA results are sharply peaked inside the MCMC, and GA-Fisher, ellipses.

## 5. Conclusions

We highlight that GA serves as a powerful optimization strategy, with hyperparameters that can be fine-tuned to achieve desired outcomes. For the purpose of cosmological parameter estimation, our goal was to localize the results around the optimal solution, enabling traditional interpretation similar to a posterior distribution. However, mastering this tuning process requires practice. We investigated the key hyperparameters of GA—fitness, mutation, and crossover—to assess their significant impact on the final results. Our findings indicate that fitness and mutation

play crucial roles in guiding the evolution toward a population that is concentrated around the optimal solution. Additionally, while we experimented with other hyperparameters such as selection rate and type, and crossover type, they did not demonstrate a substantial impact compared to the primary ones we opted to highlight in this pedagogical study.

We hope that this simple application of GA clarifies the strengths and shortcomings of the method, but most essentially why it may be considered as a promising supporting tool to MCMC for cosmological analysis. GA offers an effective way to navigate complex parameter spaces, akin to finding a needle in a haystack—while MCMC can predict where the needle may have landed, GA can directly find the needle.

Looking ahead, future work can revolve around testing GA with more complex astrophysical scenarios and cosmological models beyond curved  $\Lambda$ CDM, further exploring the reach of biology-inspired optimization in enhancing our understanding of the cosmos.

## Acknowledgements

RCB is supported by an appointment to the JRG Program at the APCTP through the Science and Technology Promotion Fund and Lottery Fund of the Korean Government, and was also supported by the Korean Local Governments in Gyeongsangbuk-do Province and Pohang City. RCB acknowledges the hospitality of the Institute of Physics, Academia Sinica that enabled the completion of this work. The initial stages of this work were done in part during the TCA Summer Student Program 2023 hosted by the NCTS Taiwan.

## References

- [1] G. Rudolph, Convergence analysis of canonical genetic algorithms, *IEEE transactions on neural networks* 5 (1) (1994) 96–101.
- [2] Y. Akrami, P. Scott, J. Edsjo, J. Conrad, L. Bergstrom, A Profile Likelihood Analysis of the Constrained MSSM with Genetic Algorithms, *JHEP* 04 (2010) 057. [arXiv:0910.3950](#), [doi:10.1007/JHEP04\(2010\)057](#).
- [3] J. Crowder, N. J. Cornish, L. Reddinger, Darwin meets Einstein: LISA data analysis using genetic algorithms, *Phys. Rev. D* 73 (2006) 063011. [arXiv:gr-qc/0601036](#), [doi:10.1103/PhysRevD.73.063011](#).
- [4] C. Bogdanos, S. Nesseris, Genetic Algorithms and Supernovae Type Ia Analysis, *JCAP* 05 (2009) 006. [arXiv:0903.2805](#), [doi:10.1088/1475-7516/2009/05/006](#).
- [5] S. Nesseris, A. Shafieloo, A model independent null test on the cosmological constant, *Mon. Not. Roy. Astron. Soc.* 408 (2010) 1879–1885. [arXiv:1004.0960](#), [doi:10.1111/j.1365-2966.2010.17254.x](#).
- [6] S. Nesseris, J. Garcia-Bellido, A new perspective on Dark Energy modeling via Genetic Algorithms, *JCAP* 11 (2012) 033. [arXiv:1205.0364](#), [doi:10.1088/1475-7516/2012/11/033](#).
- [7] R. Medel-Esquivel, I. Gómez-Vargas, A. A. M. Sánchez, R. García-Salcedo, J. Alberto Vázquez, Cosmological Parameter Estimation with Genetic Algorithms, *Universe* 10 (1) (2024) 11. [arXiv:2311.05699](#), [doi:10.3390/universe10010011](#).
- [8] E. Di Valentino, et al., The CosmoVerse White Paper: Addressing observational tensions in cosmology with systematics and fundamental physics [arXiv:2504.01669](#).
- [9] E. Di Valentino, et al., Snowmass2021 - Letter of interest cosmology intertwined I: Perspectives for the next decade, *Astropart. Phys.* 131 (2021) 102606. [arXiv:2008.11283](#), [doi:10.1016/j.astropartphys.2021.102606](#).
- [10] E. Di Valentino, et al., Snowmass2021 - Letter of interest cosmology intertwined II: The hubble constant tension, *Astropart. Phys.* 131 (2021) 102605. [arXiv:2008.11284](#), [doi:10.1016/j.astropartphys.2021.102605](#).
- [11] E. Di Valentino, et al., Cosmology intertwined III:  $f\sigma_8$  and  $S_8$ , *Astropart. Phys.* 131 (2021) 102604. [arXiv:2008.11285](#), [doi:10.1016/j.astropartphys.2021.102604](#).
- [12] N. Schöneberg, G. Franco Abellán, A. Pérez Sánchez, S. J. Witte, V. Poulin, J. Lesgourgues, The H0 Olympics: A fair ranking of proposed models, *Phys. Rept.* 984 (2022) 1–55. [arXiv:2107.10291](#), [doi:10.1016/j.physrep.2022.07.001](#).
- [13] N. Aghanim, et al., Planck 2018 results. VI. Cosmological parameters, *Astron. Astrophys.* 641 (2020) A6. [arXiv:1807.06209](#), [doi:10.1051/0004-6361/201833910](#).
- [14] A. G. Riess, et al., A Comprehensive Measurement of the Local Value of the Hubble Constant with 1 km/s/Mpc Uncertainty from the Hubble Space Telescope and the SH0ES Team, *Astrophys. J. Lett.* 934 (1) (2022) L7. [arXiv:2112.04510](#), [doi:10.3847/2041-8213/ac5c5b](#).
- [15] M. Moresco, Measuring the expansion history of the Universe with cosmic chronometers [arXiv:2412.01994](#).
- [16] D. Stern, R. Jimenez, L. Verde, M. Kamionkowski, S. A. Stanford, Cosmic chronometers: constraining the equation of state of dark energy. I:  $H(z)$  measurements, *JCAP* 2010 (2) (2010) 008. [arXiv:0907.3149](#), [doi:10.1088/1475-7516/2010/02/008](#).
- [17] M. Moresco, et al., Improved constraints on the expansion rate of the Universe up to  $z \sim 1.1$  from the spectroscopic evolution of cosmic chronometers, *JCAP* 2012 (8) (2012) 006. [arXiv:1201.3609](#), [doi:10.1088/1475-7516/2012/08/006](#).
- [18] C. Zhang, H. Zhang, S. Yuan, S. Liu, T.-J. Zhang, Y.-C. Sun, Four new observational  $H(z)$  data from luminous red galaxies in the Sloan Digital Sky Survey data release seven, *Research in Astronomy and Astrophysics* 14 (10) (2014) 1221–1233. [arXiv:1207.4541](#), [doi:10.1088/1674-4527/14/10/002](#).
- [19] M. Moresco, Raising the bar: new constraints on the Hubble parameter with cosmic chronometers at  $z \sim 2$ , *Mon. Not. Roy. Astron. Soc.* 450 (1) (2015) L16–L20. [arXiv:1503.01116](#), [doi:10.1093/mnras/1/slv037](#).

- [20] M. Moresco, L. Pozzetti, A. Cimatti, R. Jimenez, C. Maraston, L. Verde, D. Thomas, A. Citro, R. Tojeiro, D. Wilkinson, A 6% measurement of the Hubble parameter at  $z \sim 0.45$ : direct evidence of the epoch of cosmic re-acceleration, JCAP 05 (2016) 014. [arXiv:1601.01701](#), [doi:10.1088/1475-7516/2016/05/014](#).
- [21] A. L. Ratsimbazafy, S. I. Loubser, S. M. Crawford, C. M. Cress, B. A. Bassett, R. C. Nichol, P. Väisänen, Age-dating Luminous Red Galaxies observed with the Southern African Large Telescope, Mon. Not. Roy. Astron. Soc. 467 (3) (2017) 3239–3254. [arXiv:1702.00418](#), [doi:10.1093/mnras/stx301](#).
- [22] D. Brout, et al., The Pantheon+ Analysis: SuperCal-Fragilistic Cross Calibration, Retrained SALT2 Light Curve Model, and Calibration Systematic Uncertainty [arXiv:2112.03864](#).
- [23] D. Brout, et al., The Pantheon+ Analysis: Cosmological Constraints, Astrophys. J. 938 (2) (2022) 110. [arXiv:2202.04077](#), [doi:10.3847/1538-4357/ac8e04](#).
- [24] D. Scolnic, et al., The Pantheon+ Analysis: The Full Data Set and Light-curve Release, Astrophys. J. 938 (2) (2022) 113. [arXiv:2112.03863](#), [doi:10.3847/1538-4357/ac8b7a](#).
- [25] M. Moresco, Addressing the Hubble tension with cosmic chronometers [arXiv:2307.09501](#).
- [26] M. Moresco, R. Jimenez, L. Verde, L. Pozzetti, A. Cimatti, A. Citro, Setting the Stage for Cosmic Chronometers. I. Assessing the Impact of Young Stellar Populations on Hubble Parameter Measurements, Astrophys. J. 868 (2) (2018) 84. [arXiv:1804.05864](#), [doi:10.3847/1538-4357/aae829](#).
- [27] M. Moresco, R. Jimenez, L. Verde, A. Cimatti, L. Pozzetti, Setting the Stage for Cosmic Chronometers. II. Impact of Stellar Population Synthesis Models Systematics and Full Covariance Matrix, Astrophys. J. 898 (1) (2020) 82. [arXiv:2003.07362](#), [doi:10.3847/1538-4357/ab9eb0](#).
- [28] S. Perlmutter, et al., Discovery of a supernova explosion at half the age of the Universe and its cosmological implications, Nature 391 (1998) 51–54. [arXiv:astro-ph/9712212](#), [doi:10.1038/34124](#).
- [29] A. G. Riess, et al., Observational evidence from supernovae for an accelerating universe and a cosmological constant, Astron. J. 116 (1998) 1009–1038. [arXiv:astro-ph/9805201](#), [doi:10.1086/300499](#).
- [30] S. Perlmutter, et al., Measurements of  $\Omega$  and  $\Lambda$  from 42 High Redshift Supernovae, Astrophys. J. 517 (1999) 565–586. [arXiv:astro-ph/9812133](#), [doi:10.1086/307221](#).
- [31] W. L. Freedman, et al., Final results from the Hubble Space Telescope key project to measure the Hubble constant, Astrophys. J. 553 (2001) 47–72. [arXiv:astro-ph/0012376](#), [doi:10.1086/320638](#).
- [32] P. Astier, et al., The Supernova Legacy Survey: Measurement of  $\Omega_M$ ,  $\Omega_\Lambda$  and  $\Omega_\Lambda$  from the first year data set, Astron. Astrophys. 447 (2006) 31–48. [arXiv:astro-ph/0510447](#), [doi:10.1051/0004-6361:20054185](#).
- [33] A. G. Riess, et al., A 2.4% Determination of the Local Value of the Hubble Constant, Astrophys. J. 826 (1) (2016) 56. [arXiv:1604.01424](#), [doi:10.3847/0004-637X/826/1/56](#).
- [34] D. M. Scolnic, et al., The Complete Light-curve Sample of Spectroscopically Confirmed SNe Ia from Pan-STARRS1 and Cosmological Constraints from the Combined Pantheon Sample, Astrophys. J. 859 (2) (2018) 101. [arXiv:1710.00845](#), [doi:10.3847/1538-4357/aab9bb](#).
- [35] E. Pastén, V. H. Cárdenas, Testing  $\Lambda$ CDM cosmology in a binned universe: Anomalies in the deceleration parameter, Phys. Dark Univ. 40 (2023) 101224. [arXiv:2301.10740](#), [doi:10.1016/j.dark.2023.101224](#).
- [36] L. Perivolaropoulos, F. Skara, On the homogeneity of SNIa absolute magnitude in the Pantheon+ sample, Mon. Not. Roy. Astron. Soc. 520 (4) (2023) 5110–5125. [arXiv:2301.01024](#), [doi:10.1093/mnras/stad451](#).
- [37] R. Trotta, Bayes in the sky: Bayesian inference and model selection in cosmology, Contemp. Phys. 49 (2008) 71–104. [arXiv:0803.4089](#), [doi:10.1080/00107510802066753](#).
- [38] A. Lewis, [GetDist: a Python package for analysing Monte Carlo samples](#) [arXiv:1910.13970](#).  
URL <https://getdist.readthedocs.io>
- [39] J. Torrado, A. Lewis, Cobaya: Code for Bayesian Analysis of hierarchical physical models, arXiv e-prints (2020) arXiv:2005.05290 [arXiv:2005.05290](#).
- [40] D. Foreman-Mackey, D. W. Hogg, D. Lang, J. Goodman, emcee: The MCMC Hammer, Publ. Astron. Soc. Pac. 125 (2013) 306–312. [arXiv:1202.3665](#), [doi:10.1086/670067](#).
- [41] R. C. Bernardo, J. Levi Said, Towards a model-independent reconstruction approach for late-time Hubble data, JCAP 08 (2021) 027. [arXiv:2106.08688](#), [doi:10.1088/1475-7516/2021/08/027](#).
- [42] I. Gómez-Vargas, J. B. Andrade, J. A. Vázquez, Neural networks optimized by genetic algorithms in cosmology, Phys. Rev. D 107 (4) (2023) 043509. [arXiv:2209.02685](#), [doi:10.1103/PhysRevD.107.043509](#).
- [43] M. B. Bainbridge, J. K. Webb, Artificial intelligence applied to the automatic analysis of absorption spectra. Objective measurement of the fine structure constant, Mon. Not. Roy. Astron. Soc. 468 (2) (2017) 1639–1670. [arXiv:1606.07393](#), [doi:10.1093/mnras/stx179](#).
- [44] M. B. Bainbridge, J. K. Webb, Evaluating the New Automatic Method for the Analysis of Absorption Spectra Using Synthetic Spectra, Universe 3 (2) (2017) 34. [arXiv:1704.08710](#), [doi:10.3390/universe3020034](#).
- [45] C.-C. Lee, J. K. Webb, R. F. Carswell, D. Milaković, Artificial intelligence and quasar absorption system modelling; application to fundamental constants at high redshift, Mon. Not. Roy. Astron. Soc. 504 (2) (2021) 1787–1800. [arXiv:2008.02583](#), [doi:10.1093/mnras/stab977](#).
- [46] J. K. Webb, C.-C. Lee, R. F. Carswell, D. Milaković, Getting the model right: an information criterion for spectroscopy, Mon. Not. Roy. Astron. Soc. 501 (2) (2021) 2268–2278. [arXiv:2009.08336](#), [doi:10.1093/mnras/staa3551](#).
- [47] A. Fawzy Gad, Pygad: an intuitive genetic algorithm python library, Multimed. Tools Appl. 83 (2023) 58029–58042. [arXiv:2106.06158](#), [doi:10.1007/s11042-023-17167-y](#).